Langmuir
Article
pubs.acs.org/Langmuir

Morphology Controlled Surface-Assisted Self-Assembled Microtube Junctions and Dendrites of Metal Free Porphyrin-Based Semiconductor

Pan Ma,[†] Yanli Chen,[§] Yongzhong Bian,[†] and Jianzhuang Jiang*[,†,‡]

[†]*Department of Chemistry, Shandong University, Jinan 250100, China,* [‡]*Department of Chemistry, University of Science and Technology Beijing, Beijing 100083, China, and* [§]*Department of Chemistry, University of Jinan, Jinan 250022, China*

Received August 24, 2009. Revised Manuscript Received October 27, 2009

Solution-vapor annealing of drop-cast thin films of *meso*-5,10,15,20-tetra-*n*-decylporphyrin $H_2T(C_{10}H_{21})_4P$ deposited on SiO_2 substrate and quartz leads to the formation of well-defined self-assemblies. Their self-assembling properties in *n*-hexane vapor and chloroform vapor were comparatively investigated by scanning electron microscopy (SEM), X-ray diffraction (XRD) technique, and IR and UV−vis spectroscopy. Intermolecular $\pi-\pi$ interaction in cooperation with the van der Waals interaction of metal free porphyrin and solvent−solute interaction leads to the formation of microleaves and microtube dendrites in *n*-hexane vapor and chloroform vapor, respectively. Electronic absorption spectroscopic data on the self-assembled microstructures reveal the *J*-aggregate nature in both the microleaves and microtube dendrites. However, the difference in the shift of the Soret and Q bands for the two kinds of aggregates relative to corresponding solution absorption bands indicates the dependence of the solvent−porphyrin molecular interaction during the annealing self-assembly process, which counterbalances the intermolecular interactions, particularly the hydrophobic interaction between side chains. IR and XRD results clearly reveal the higher molecular ordering nature of microtube dendrites than that of microleaves, further confirming the effect of the solvent on tuning the intermolecular interaction and in turn the molecular packing mode in aggregates of porphryin compounds. The present results appear to represent the first example of orderly micrometer-sized tube junctions and dendrites of porphyrin prepared through a self-assembly process, providing an effective and new method toward the synthesis of complicated nanotubular structures. In addition, micrometer-sized leaves and tube dendrites were revealed to show good semiconductor features. Highly reproducible and sensitive gas response characteristics have also been observed in these microstructures.

Introduction

Various kinds of micro- and nanotubes have attracted increasing attention since the discovery of carbon nanotubes (CNTs) by Iijima in 1991 owing to their attractive diverse potential applications ranging from nanoelectronics to biomedical devices.[1,2] Recently, much more research interest has been given to nanotubes formed from a variety of materials including C_{60}, metals, inorganic compounds, and polymers prepared using different preparation methods including hydrothermal synthesis, self-assembly, surfactant-assisted synthesis, and template synthesis.[3−6] In fact, the vessels in the bodies of animals and in plants are also composed of tubes, and their junctions often exist in a dendritic morphology.[7] Nevertheless, nanotube junctions as well as individual nanotubes have been revealed to play a key role in nanoelectronic devices.[8] With this aim in mind, carbon nanotube junctions prepared by chemical vapor deposition (CVD), template pathway, and by joining two individual nanotubes were investigated.[9]

On the other hand, tetrapyrrole derivatives including porphyrins and phthalocyanines have been extensively and intensively investigated as advanced molecular materials.[10] This class of compounds usually exhibits strong $\pi-\pi$ intramolecular interaction, resulting in intriguing electronic and optical properties and potential applications as gas sensors and organic field-effect transistors (OFETs).[11] Among all the related investigation

*Corresponding author. E-mail: jzjiang@sdu.edu.cn, jianzhuang@ustb.edu.cn.

(1) (a) Iijima, S. *Nature* **1991**, *354*, 56–58. (b) Dekker, C. *Phys. Today* **1999**, *52*, 22–28.

(2) (a) Wei, Z. X.; Zhang, L. J.; Yu, M.; Yang, Y. S.; Wan, M. X. *Adv. Mater.* **2003**, *15*, 1382–1385. (b) Lei, J.; Menon, V. P.; Martin, C. R. *Polym. Adv. Technol.* **1992**, *4*, 124–132.

(3) (a) Hu, J.; Odom, T. W.; Lieber, C. M. *Acc. Chem. Res.* **1999**, *32*, 435–445. (b) Jérôme, C.; Demoustier-Champagne, S.; Legras, R.; Jérôme, R. *Chem.—Eur. J.* **2000**, *6*, 3089–3093. (c) Patzke, G. R.; Krumeich, F.; Nesper, R. *Angew. Chem., Int. Ed.* **2002**, *41*, 2446–2461. (d) Zelenski, C. M.; Dorhout, P. K. *J. Am. Chem. Soc.* **1998**, *120*, 734–742.

(4) (a) Martin, C. R. *Science* **1994**, *266*, 1961–1966. (b) Liu, H.; Li, Y.; Jiang, L.; Luo, H.; Xiao, S.; Fang, H.; Li, H.; Zhu, D.; Yu, D.; Xu, J.; Xiang, B. *J. Am. Chem. Soc.* **2002**, *124*, 13370–13371. (c) Lee, J.; Koh, W.; Chae, W.; Kim, Y. *Chem. Commun.* **2002**, 138–139. (d) Kyotani, T.; Tsai, L.; Tomita, A. *Chem. Mater.* **1996**, *8*, 2109–2113.

(5) Steinhart, M.; Wendorff, J. H.; Greiner, A.; Wehrspohn, R. B.; Nielsch, K.; Schilling, J.; Choi, J.; Gösele, U. *Science* **2002**, *296*, 1997.

(6) (a) Schnur, J. M. *Science* **1993**, *262*, 1669–1676. (b) Shimizu, T.; Masuda, M.; Minamikawa, H. *Chem. Rev.* **2005**, *105*, 1401–1443. (c) Hu, J.; Guo, Y.; Liang, H.; Wan, L.; Jiang, L. *J. Am. Chem. Soc.* **2005**, *127*, 17090–17095. (d) Steinhart, M.; Wehrspohn, R. B.; Gösele, U.; Wendorff, J. H. *Angew. Chem., Int. Ed.* **2004**, *43*, 1334–1344.

(7) Mandelbrot, B. B. *The Fractal Geometry of Nature*; Freeman: San Francisco, CA, 1982.

(8) (a) Menon, M.; Srivastava, D. *Phys. Rev. Lett.* **1997**, *79*, 4453–4456. (b) Treboux, G.; Lapstun, P.; Silverbrool, K. *Chem. Phys. Lett.* **1999**, *306*, 402–406. (c) Andriotis, A. N.; Menon, M.; Srivastava, D.; Chernozatonskii, L. *Phys. Rev. Lett.* **2001**, *87*, 066802.

(9) (a) Terrones, M.; Banhart, F.; Grobert, N.; Charlier, J.-C.; Terrones, H.; Ajayan, P. M. *Phys. Rev. Lett.* **2002**, *89*, 075505. (b) Ting, J.-M.; Chang, C.-C. *Appl. Phys. Lett.* **2002**, *80*, 324–325. (c) Satishkumar, B. C.; Thomas, P. J.; Govindaraj, A.; Rao, C. N. R. *Appl. Phys. Lett.* **2002**, *77*, 2530–2532.

(10) (a) Kirin, I. S.; Moskalev, P. N.; Makashev, Y. A. *Russ. J. Inorg. Chem.* **1965**, *10*, 1065. (b) Ng, D. K. P.; Jiang, J. *Chem. Soc. Rev.* **1997**, *26*, 433–442. (c) Buchler, J. W.; Ng, D. K. P. In *The Porphyrin Handbook*; Kadish, K. M., Smith, K. M., Guilard, R., Eds.; Academic Press: San Diego, 2000; Vol. *3*, pp 245−294.(d) Jiang, J.; Kasuga, K.; Arnold, D. P. In *Supramolecular Photo-sensitive and Electro-active Materials*; Nalwa, H. S., Ed.; Academic Press: New York, 2001; pp 113−210.

(11) (a) Bian, Y.; Jiang, J.; Tao, Y.; Choi, M. T. M.; Li, R.; Ng, A. C. H.; Zhu, P.; Pan, N.; Sun, X.; Arnold, D. P.; Zhou, Z.-Y.; Li, H.-W.; Mak, T. C. W.; Ng, D. P. K. *J. Am. Chem. Soc.* **2003**, *125*, 12257–12267. (b) Su, W.; Jiang, J.; Xiao, K.; Chen, Y.; Zhao, Q. *Langmuir* **2005**, *21*, 6527–6531. (c) Chen, Y.; Su, W.; Bai, M.; Jiang, J.; Li, X.; Liu, Y.; Wang, L.; Wang, S. *J. Am. Chem. Soc.* **2005**, *127*, 15700–15701.

Scheme 1. Molecular Structure of $H_2T(C_{10}H_{21})_4P$

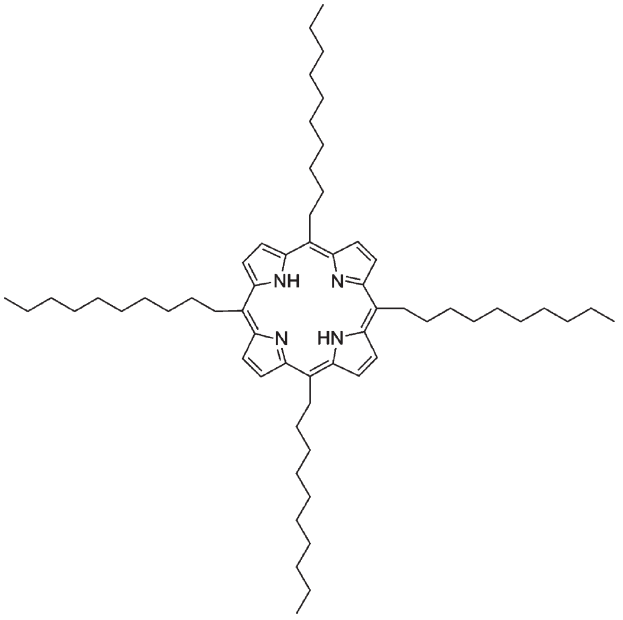

toward applications, one focus is the fabrication and preparation of designable assemblies and nano/micromaterials.[12−15] Recently, a composite porphyrin nanotube was produced by electrostatic force between two oppositely charged monomeric porphyrin compounds, for which the photocatalytic activity to reduce aqueous metal cations was also demonstrated.[13] According to Müllen and co-workers, nanotubes of monomeric naphthalocyaninato nickel complex were also successfully fabricated by a template method.[15a] These results seem to represent the most important achievement toward utilization of porphyrin/phthalocyanine nanotubes.[13b,14,16] Although micro- and nanotubes of porphyrins have been prepared by template synthesis[17] and self-assembly procedures,[18] reports concerning the micro- or nanotube junctions, especially complicated junctions with dendritic morphology, remain rare.

In the present article, we describe the preparation and characterization of microleaves and microtube dendrites and their junctions of metal free *meso*-5,10,15,20-tetra-*n*-decylporphyrin, $H_2T(C_{10}H_{21})_4P$ (Scheme 1) prepared using a self-assembly process for the first time.

Experimental Section

Measurements. IR spectra were recorded as KBr pellets using a Bio-Rad FTS-165 spectrometer with 2 cm^{-1} resolution. Electronic absorption spectra were recorded on a Hitachi U-4100 spectrophotometer. Scanning electron microscopy (SEM) images were obtained using a HITACHI S-520 scanning electron microscope. For SEM imaging, Au (1−2 nm) was sputtered onto the substrate to prevent charging effects and to improve the image clarity. Morphology examination by atomic force microscopy (AFM) imaging was carried out on a Veeco Nanoscope Multimode III SPM instrument with taping mode. X-ray diffraction (XRD) experiments were carried out on a Rigaku D/max-γB X-ray diffractometer. Substrates used in the present study were successively cleaned with pure water, acetone, and ethanol.

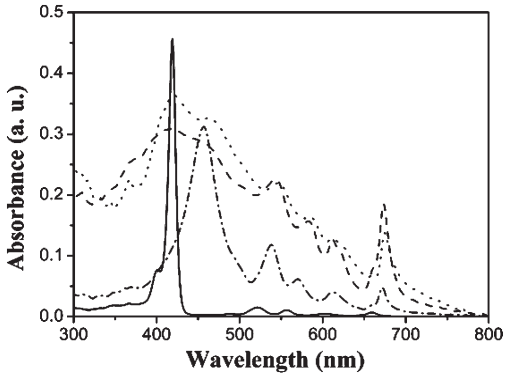

Figure 1. Electronic absorption spectra of metal free porphyrin in $CHCl_3$ solution (solid line) and its microleaves from *n*-hexane-vapor annealing (dotted line), microtube dendrites from chloroform-vapor annealing (dashed line) and drop-cast film (dash dotted line).

Solvent-Vapor Annealing. The sample, typically a thin film, was prepared by drop-casting a concentrated chloroform solution of $H_2T(C_{10}H_{21})_4P$ (6 mg/mL) onto SiO_2 or quartz substrate. The solvent-vapor annealing was carried out in a desiccator having a lid with a valve-controlled vent, which was connected to a vacuum pump. About 30 mL of solvent in a beaker was put in the chamber, followed by vacuum-pumping for about 5 min. The chamber was then sealed by closing the vent, leading to saturation of the solvent vapor inside the chamber. The sample was kept in the vapor environment for 24 h to complete the annealing process. When switching between different solvents, the chamber was cleaned by repeated vacuum pumping (about three times) before putting in a new beaker of solvent.

Device Fabrication. The Au electrodes were thermally evaporated onto the ordered microstructures by use of a micrometer-sized Au wire as the mask. These electrodes have a channel length (L) of 55 μm. The current−voltage characteristics were obtained with a Keithley 4200 semiconductor characterization system at room temperature in air.

Chemicals. All reagents and solvents were used as received. Metal free porphyrin with four *n*-decyl groups at the *meso* positions of porphyrin ring, namely, $H_2T(C_{10}H_{21})_4P$, was prepared according to a literature procedure.[19]

Results and Discussion

Electronic Absorption Spectra. The electronic absorption spectrum of the porphyrin derivative $H_2T(C_{10}H_{21})_4P$ in $CHCl_3$ was recorded, and the data are compiled in Table S1 (Supporting Information) and Figure 1. As expected, $H_2T(C_{10}H_{21})_4P$ shows typical features of a metal free porphyrin compound in its electronic absorption spectrum, revealing the nonaggregated molecular spectroscopic nature of this metal free porphyrin compound in $CHCl_3$. In line with H_2TPP (H_2TPP = 5,10,15,20-tetraphenyl-porphyrin),[20] the absorption around 419 nm for $H_2T(C_{10}H_{21})_4P$ can be attributed to the porphyrin Soret band,

(12) Gong, X.; Milic, T.; Xu, C.; Batteas, J. D.; Drain, C. M. *J. Am. Chem. Soc.* **2002**, *124*, 14290–14291.
(13) (a) Wang, Z.; Medforth, C. J.; Shelnutt, J. A. *J. Am. Chem. Soc.* **2004**, *126*, 15954–15955. (b) Wang, Z.; Medforth, C. J.; Shelnutt, J. A. *J. Am. Chem. Soc.* **2004**, *126*, 16720–16721.
(14) (a) Nitschke, C.; Flaherty, S.; Kro1ll, M.; Blau, W. *J. Phys. Chem. B* **2004**, *108*, 1287–1295. (b) Jenekhe, S. A.; Yi, S. *J. Adv. Mater.* **2000**, *12*, 1274–1278. (c) Zhang, X.; Wang, Y.; Ma, Y.; Ye, Y.; Wang, Y.; Wu, K. *Langmuir* **2006**, *22*, 344–348.
(15) (a) Zhi, L.; Gorelik, T.; Wu, J.; Kolb, U.; Müllen, K. *J. Am. Chem. Soc.* **2005**, *127*, 12792–12793. (b) Zhi, L.; Wu, J.; Li, J.; Kolb, U.; Müllen, K. *Angew. Chem., Int. Ed.* **2005**, *44*, 2120–2123.
(16) (a) Tang, Q.; Li, H.; He, M.; Hu, W.; Liu, C.; Chen, K.; Wang, C.; Liu, Y.; Zhu, D. *Adv. Mater.* **2006**, *18*, 65–68. (b) Cao, L.; Chen, H.; Zhou, H.; Zhu, L.; Sun, J.; Zhang, X.; Xu, J.; Wang, M. *Adv. Mater.* **2003**, *15*, 909–913.
(17) Liu, Q.; Li, Y.; Liu, H.; Chen, Y.; Wang, X.; Zhang, Y.; Li, X.; Jiang, J. *J. Phys. Chem. C* **2007**, *111*, 7298–7301.
(18) Huang, C.; Wen, L.; Liu, H.; Li, Y.; Liu, X.; Yuan, M.; Zhai, J.; Jiang, L.; Zhu, D. *Adv. Mater.* **2009**, *21*, 1721–1725.
(19) Ma, P.; Chen, Y.; Sheng, N.; Bian, Y.; Jiang, J. *Eur. J. Inorg. Chem.* **2009**, 954–960.
(20) Ulman, A.; Manassen, J. *J. Am. Chem. Soc.* **1975**, *97*, 6540–6544.

while the four typical weak absorptions at 521, 557, 601, and 659 nm are attributed to the metal free porphyrin Q bands (Figure 1). The electronic absorption spectra of the aggregates annealed in chloroform and *n*-hexane vapor, respectively, of this compound are also given in Figure 1, which are significantly different from the spectrum of $H_2T(C_{10}H_{21})_4P$ dissolved in $CHCl_3$. Obvious band broadening was observed due to the effect of the closely compacted molecular assembly. Unlike the drop-cast film with only one broad Soret band, both the microleaves and microtube dendrites show a split and broadened Soret band with the gravity center at the lower energy side in comparison with the Soret band of $H_2T(C_{10}H_{21})_4P$ dissolved in $CHCl_3$ probably due to exciton coupling between the adjacent porphyrin units.[21] Compared to the chloroform solution spectrum, the absorptions of both aggregates annealed in *n*-hexane and in chloroform vapor are red-shifted, indicating the formation of J aggregates in the molecular assembly of $H_2T(C_{10}H_{21})_4P$ due to the strong exciton coupling.[22] However, the shift degree of the Soret and Q bands in the absorption spectra of the two kinds of aggregates of H_2T-$(C_{10}H_{21})_4P$ is different (Table S1 (Supporting Information) and Figure 1), showing a dependence on the solvent−porphyrin molecule interaction during the annealing self-assembly process, which counterbalances the intermolecular interactions, particularly the hydrophobic interaction between side chains.[23] The result suggests the significant effect of the solvent on the intermolecular interaction in the annealing self-assembly process of the prophyrin compound. Further evidence comes from XRD experimental results, SEM observation, and infrared spectroscopy as detailed below.

X-ray Diffraction Patterns. The microstructures were fabricated by solvent-vapor annealing of the drop-cast thin films of the compound. The internal structure of self-assembled microstructures was investigated by XRD analysis (Figure 2). As shown in Figure 2A, in the low angle range, the XRD diagram of the aggregates formed from *n*-hexane-vapor annealing shows a strong refraction peak at $2\theta = 4.12°$ (corresponding to 2.14 nm) ascribed to the refraction from the (100) plane constructed by the porphyrin layers. In addition, the XRD pattern displays two well-defined peaks at the wide angle XRD pattern corresponding to the distances at 0.63 and 0.31 nm that relate to the liquidlike order of the peripheral alkyl chains and the stacking distance between tetrapyrrole cores of neighboring monomeric molecules along the direction perpendicular to the tetarpyrrole rings, respectively.[24]

As shown in Figure 2B, the XRD diagram of the aggregates formed from chloroform-vapor annealing shows two strong peaks at 2.14 and 2.45 nm, respectively, which are ascribed to the refractions from the (100) and (001) planes related to the distances between porphyrin columns.[25] These diffraction results could be assigned to the refractions from a rectangular lattice with the cell parameters of $a = 2.14$ nm and $c = 2.45$ nm. In addition, the XRD pattern also displays four weaker higher order refractions at 1.06, 0.71, 0.53, and 0.43 nm, which are ascribed to the refractions from the (200), (300), (400), and (500) planes,

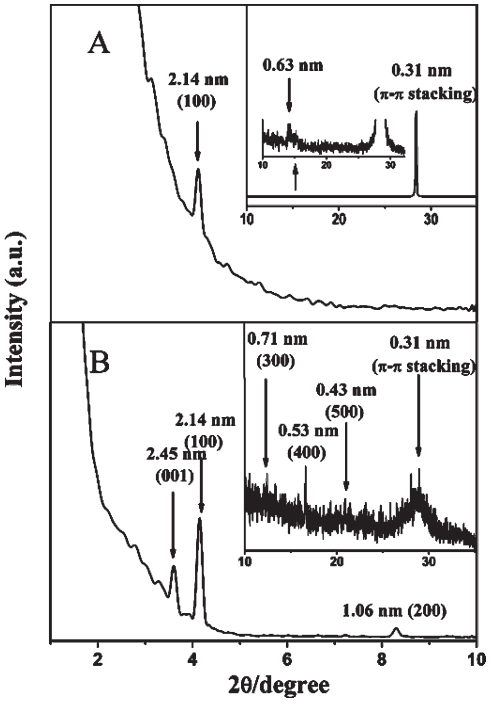

Figure 2. X-ray powder diffraction patterns of compound H_2T-$(C_{10}H_{21})_4P$: (A) microleaves from *n*-hexane-vapor annealing; (B) microtube dendrites from chloroform-vapor annealing.

respectively, revealing the high molecular ordering nature of this microstructure along the *a*-axis of the unit cell. It therefore could be concluded that $H_2T(C_{10}H_{21})_4P$ molecules self-assemble to form a higher ordered crystalline film with a unique internal structure in the aggregates based on chloroform-vapor annealing than that by *n*-hexane-vapor annealing, confirming again the effect of the solvent on tuning the intermolecular interaction and in turn the molecular packing mode in aggregates due to different interactions between porphyrin and solvent molecules during the annealing self-assembly process of this porphryin derivative. It is worth noting that, in the wide angle region, the microstructures formed from chloroform-vapor annealing also present an additional refraction at 0.31 nm due to the stacking distance between tetrapyrrole cores of $H_2T(C_{10}H_{21})_4P$ molecules along the direction perpendicular to the tetarpyrrole rings.[26]

Morphology of the Aggregates. The morphology of the aggregates was examined by SEM. Samples to be annealed were prepared by drop-casting a 6 mg/mL chloroform solution of $H_2T(C_{10}H_{21})_4P$ onto the surface of SiO_2 substrate or quartz. The SEM images of aggregates of $H_2T(C_{10}H_{21})_4P$ are shown in Figure 3. As shown in Figure 3C, depending mainly on the intermolecular $\pi-\pi$ interaction in cooperation with the van der Waals interaction, $H_2T(C_{10}H_{21})_4P$ molecules self-assemble into one-dimensional (1D) microstructures with leaf morphology with several micrometer long and 300−500 nm width after annealing in the vapor of *n*-hexane. In combination with the UV−vis and XRD analysis results, it could be proposed that the leaflike object is formed by the porphyrin disks in a "side-by-side" arrangement along the *a*-axis, which constructs the longitudinal direction of the

(21) Kim, Y. H.; Jeong, D. H.; Kim, D.; Jeoung, S. C.; Cho, H. S.; Kim, S. K.; Aratani, N.; Osuka, A. *J. Am. Chem. Soc.* **2001**, *123*, 76–86.
(22) Kasha, M.; Rawls, H. R.; EI-Bayoumi, M. A. *Pure Appl. Chem.* **1965**, *11*, 371–392.
(23) Balakrishnan, K.; Datar, A.; Naddo, T.; Huang, J.; Oitker, R.; Yen, M.; Zhao, J.; Zang, L. *J. Am. Chem. Soc.* **2006**, *128*, 7390–7398.
(24) Minch, B. A.; Xia, W.; Donley, C. L.; Hernandez, R. M.; Carter, C.; Carducci, M. D.; Dawson, A.; O'Brien, D. F.; Armstrong, N. R. *Chem. Mater.* **2005**, *17*, 1618–1627.
(25) Shirakawa, M.; Kawano, S.-I.; Fujita, N.; Sada, K.; Shinkai, S. *J. Org. Chem.* **2003**, *68*, 5037–5044.
(26) (a) Kimura, M.; Muto, T.; Takimoto, H.; Wada, K.; Ohta, K.; Hanabusa, K.; Shirai, H.; Kobayash, N. *Langmuir* **2000**, *16*, 2078–2082. (b) Kimura, M.; Kuroda, T.; Ohta, K.; Hanabusa, K.; Shirai, H.; Kobayashi, N. *Langmuir* **2003**, *19*, 4825–4830. (c) Minch, B. A.; Xia, W.; Donley, C. L.; Hernandez, R. M.; Carter, C.; Carducci, M. D.; Dawson, A.; O'Brien, D. F.; Armstrong, N. R. *Chem. Mater.* **2005**, *17*, 1618–1627. (d) Belarbi, Z.; Sirlin, C.; Simon, J.; Andre, J. J. *J. Phys. Chem.* **1989**, *93*, 8105–8110. (e) Kimura, M.; Wada, K.; Ohta, K.; Hanabusa, K.; Shirai, H.; Kobayashi, N. *J. Am. Chem. Soc.* **2001**, *123*, 2438–2439.

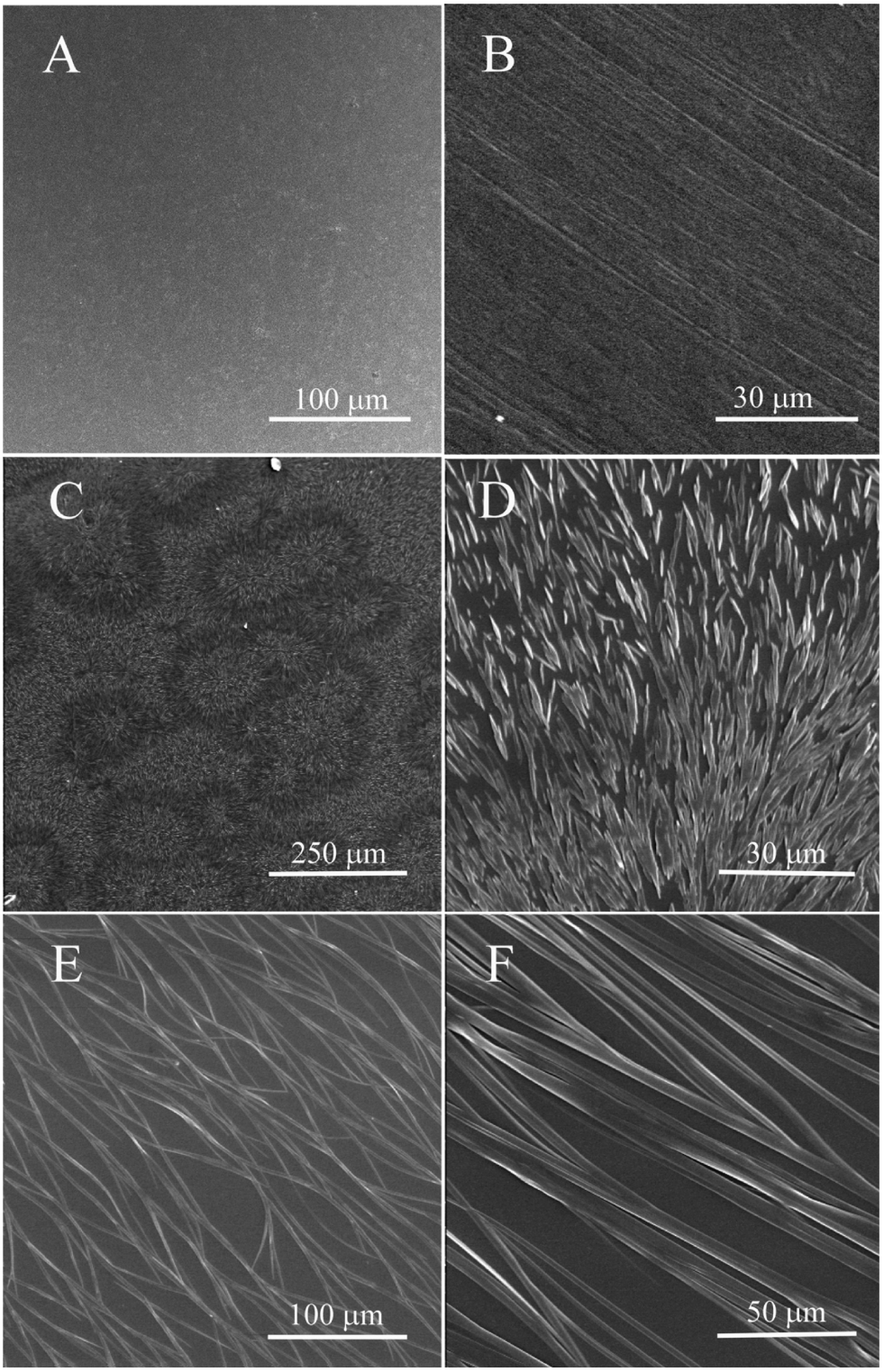

Figure 3. (A) Low-magnification field-emission scanning electron microscopy (FESEM) image of drop-cast film. (B) FESEM image of drop-cast film at high magnification. (C) Low-magnification FESEM image of microleaves from *n*-hexane-vapor annealing. (D) FESEM image of microleaves from *n*-hexane-vapor annealing at high magnification. (E) Low-magnification FESEM image of microtube dendrites from chloroform-vapor annealing. (F) FESEM image of microtube dendrites from chloroform-vapor annealing at high magnification.

microleaves (Figure 4B). On the other hand, metal free porphyrin molecules are stacked along the *b*-axis depending on the intermolecular $\pi-\pi$ interaction, leading to a separation between the neighboring metal free porphyrin rings, 0.31 nm, which is comparable with those reported for other porphyrins.[27] The long alkyl chains are interdigitated to hold the multilayer structure along the *c*-axis, which is confirmed by IR spectroscopy as detailed below. After annealing in the vapor of chloroform, $H_2T(C_{10}H_{21})_4P$ molecules self-assemble into microtubes (Figure 3E). The outer diameter of the tubes decreases from 6.9 to 0.12 μm along the longitudinal direction of the tube, and the

(27) Gao, Y.; Zhang, X.; Ma, C.; Li, X.; Jiang, J. *J. Am. Chem. Soc.* **2008**, *130*, 17044–17052.

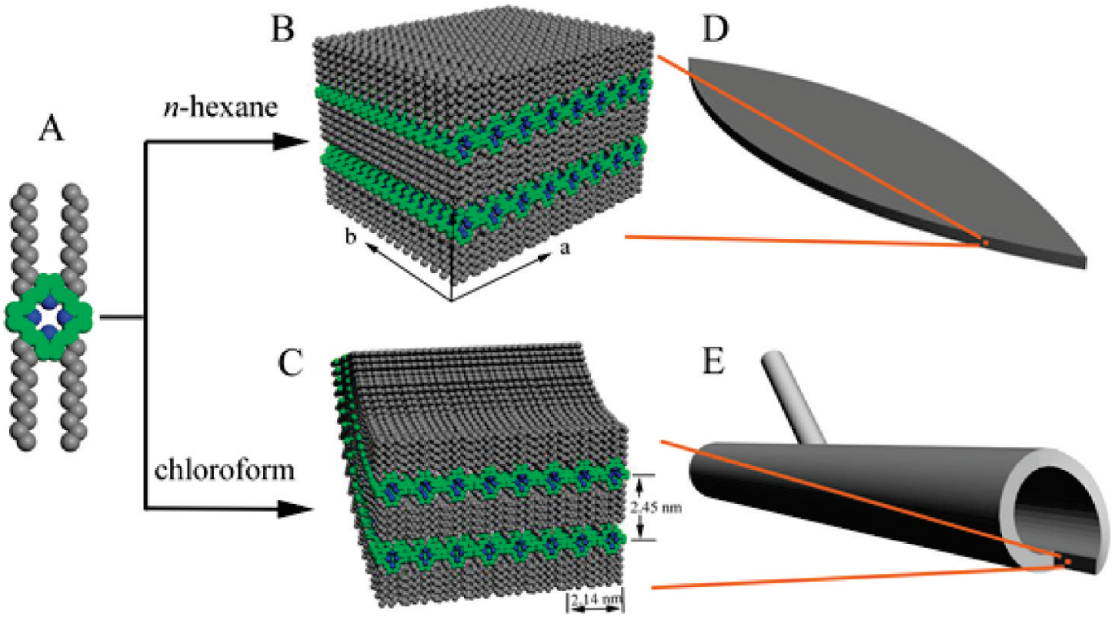

Figure 4. Schematic illustration of the proposed mechanism for the formation of microleave and microtube dendrites. (A) Space-filling model of $H_2T(C_{10}H_{21})_4P$. (B, C) Schematic representation of the microstructure wall. (D, E) Schematic representation of the microstructure. Molecular layer of porphyrin disk (green) with N atoms (blue).

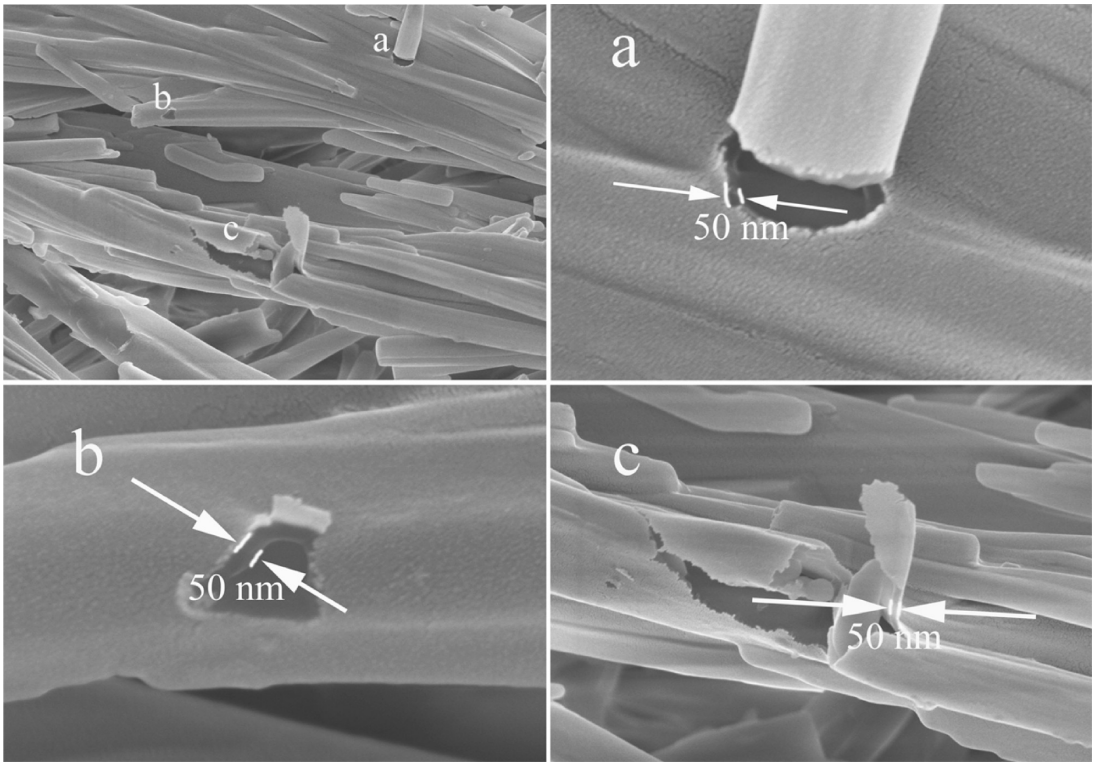

Figure 5. SEM images of microtube dendrites of compound $H_2T(C_{10}H_{21})_4P$ from chloroform-vapor annealing.

wall thickness is about 50 nm (Figure 5). The microtubes formed from $H_2T(C_{10}H_{21})_4P$ display uniform orientation, suggesting greater intermolecular order. This is favorable for the device application in photovoltaics and field effect transistors.[28] Two submicrometer-sized tubes are often linked together to form Y-junctions,[29] which in turn construct more complicated junctions, for instance, the dendrite composed of submicrometer-sized tube branches. These are similar to the vessels in the bodies of animals and in plants.[7] In addition, these submicrometer-sized tube dendrites further aggregate to form bigger dendrites, in which each submicrometer-sized tube spreads out from its root and acts as a branch. It is worth noting that the size- as well as morphology-adjustable nano/microstructures are highly desired for fabricating nano/microscale molecular (opto)-electronic devices which often require a wide variety of channel

(28) Babel, A.; Jenekhe, S. A. *J. Am. Chem. Soc.* **2005**, *125*, 13656–13657.
(29) Guo, S.; Wang, E. *Langmuir* **2008**, *24*, 2128–2132.

lengths to achieve the optimum gate or optical modulation. In the vapor of chloroform, metal free porphyrin $H_2T(C_{10}H_{21})_4P$ forms microtube dendrites with a curved 2D wall. The tubular object is considered to be formed by the rolling up of a higher ordered layer-by-layer crystalline film with a unique aggregate structure composed of π-stacked $H_2T(C_{10}H_{21})_4P$ (Figure 4). According to the molecular structure and dimensions of $H_2T(C_{10}H_{21})_4P$ molecules, the wall thickness of the tube dendrites, 50 nm, suggests a multilayer structure of the precursor tape. In addition, the long alkyl chains are interdigitated to hold the multilayer structure. These observations allow us to conclude that porphyrin disks form the curved 2D wall as the self-assembling component and the long alkyl chain parts cover the inner and outer surfaces of the curved 2D wall (Figure 4), in line with those reported previously.[15,30]

IR Spectra. The IR spectra of the microleaves and microtube dendrites being removed from the substrate are compared in Figure S1 (Supporting Information). The microtube dendrites showed CH_2 stretching vibrations at 2918 cm^{-1} (antisymmetric stretching frequency) and 2849 cm^{-1} (symmetric stretching frequency), which are almost the same as those reported,[31] indicating that the long alkyl chains are stretched to form a multilayer tape via interdigitation.[32] However, the microleaves showed a shift of the IR peak position to higher wave numbers, 2923 and 2853 cm^{-1}, indicating the relatively lower degree of ordering of the long alkyl chains in this microstructure.[33]

***I*−*V* Properties.** The uniform well-defined $H_2T(C_{10}H_{21})_4P$ microleaves and microtube dendrites fabricated would be promising candidates for applications in electronic devices through the combination of $\pi-\pi$ stacking interactions between large aromatic planes with van der Waals interactions between the long alkyl chains. To demonstrate the potentials of these microstructures, these uniform well-defined microstructures were carefully pressed onto two 55 μm spaced Au electrodes, to measure their current−voltage characteristics (Figure S2, Supporting Information).

Figures 6 and S3 (Supporting Information) show the current−voltage (*I*−*V*) characteristics of microleaves, microtube dendrites, and drop-cast films of $H_2T(C_{10}H_{21})_4P$ in the presence and absence of iodine vapor. For the devices measured, in the absence of iodine vapor, the conductivity of the drop-cast film, the microleaves, and the microtube dendrites extracted from the quasilinear region at low bias (up to −50 V) was about 9.8×10^{-7}, 1.5×10^{-6}, and 8.1×10^{-6} S m^{-1}, respectively. The improved conductive capability of microleaves might be due to the 1D $\pi-\pi$ stacking structure which favors the conductivity through side-by-side intermolecular π-delocalization, and the dramatically improved conductive capability of the microtube dendrites might be due to higher ordered crystalline molecular arrangement.

Chemical doping is usually used to tune the transistor property of a conducting organic semiconductor.[34] As a result, dozens of individual $H_2T(C_{10}H_{21})_4P$ drop-cast films, microleaves, and microtubes were prepared to examine their semiconductivity

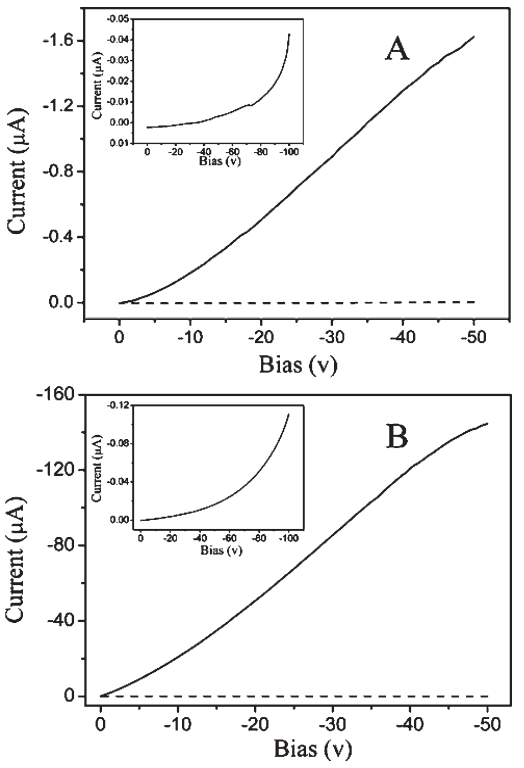

Figure 6. *I*−*V* curves measured on $H_2T(C_{10}H_{21})_4P$ microleaves (A) and microtube dendrites (B): undoped (dashed line) and doped with iodine vapor for 15 min (solid line). Inset is the *I*−*V* curve of undoped microstructures from 0 to −100 V.

changes after iodine doping. Iodine is a strong oxidative reagent that is capable of obtaining an electron from the microstructures through ground-state redox reaction (iodine, $E^{\circ}_{red} = -0.21$ V, vs SCE; $H_2T(C_{10}H_{21})_4P$, $E^{\circ}_{ox} = +0.84$ V, vs SCE). Under an applied bias, the doped electrons will rapidly migrate along the long axis of the microstructures, leading to significant enhancement in current. The conductivity of iodine-doped drop-cast films was estimated at around 3.9×10^{-6} S m^{-1}, which is not improved much compared with undoped ones, probably due to the low order and connectivity of the films as can be seen from the SEM images in Figures 3 and S5 (Supporting Information). However, the maximal conductivity of microleaves and microtube dendrites obtained with iodine dopings was estimated at around 7.9×10^{-4} and 7.1×10^{-2} S m^{-1}, respectively, which is an increase of about 3 orders and over 4 orders of magnitude in comparison with the microleaves and microtubes without exposure to the saturated vapor of iodine. It is worth noting that the conductivity of the iodine-doped microtube dendrites is more than 1 order of magnitude higher than that of undoped silicon,[35] implying the significant effect of the intermolecular interaction and the molecular packing mode in aggregates associated with the solvent−porphyrin molecular interaction on the conductivity of the microstructures. These structures with such high current modulation, along with the ultralong length, could be useful for a wide range of electronic and sensor devices. The efforts to explore such opportunities are underway.

Conclusion

Micrometer-sized tube junctions and dendrites of metal free porphyrin were synthesized through a simple solvent annealing

(30) (a) Steinhart, M.; Zimmermann, S.; Goring, P.; Schaper, A. K.; Gosele, U.; Weder, C.; Wendorff, J. H. *Nano Lett.* **2005**, *5*, 429–434. (b) Hurt, R.; Krammer, G.; Crawford, G.; Jian, K.; Rulison, C. *Chem. Mater.* **2002**, *14*, 4558–4565. (c) Jian, K.; Shim, H.-S.; Schwartzman, A.; Crawford, G. P.; Hurt, R. H. *Adv. Mater.* **2003**, *15*, 164–167.

(31) Porter, M. D.; Bright, T. B.; Allara, D. L.; Chidseyin, C. E. D. *J. Am. Chem. Soc.* **1987**, *109*, 3559–3568.

(32) (a) Hill, J. P.; Jin, W.; Kosaka, A.; Fukushima, T.; Ichihara, H.; Shimomura, T.; Ito, K.; Hashizume, T.; Ishii, N.; Aida1, T. *Science* **2004**, *304*, 1481–1483. (b) Yamamoto, Y.; Fukushima, T.; Suna, Y.; Ishii, N.; Saeki, A.; Seki, S.; Tagawa, S.; Taniguchi, M.; Kawai, T.; Aida1, T. *Science* **2006**, *314*, 1761–1764.

(33) Nakanishi, T.; Ohtani, B.; Uosaki, K. *J. Phys. Chem. B* **1998**, *102*, 1571–1577.

(34) Liu, W.; Cui, Z.-M.; Liu, Q.; Yan, D.-W.; Wu, J.-Y.; Yan, H.-J.; Guo, Y.-L.; Wang, C.-R.; Song, W.-G.; Liu, Y.-Q.; Wan, L. J. *J. Am. Chem. Soc.* **2007**, *129*, 12922–12923.

(35) Serway, R. A. *Principles of Physics*, 2nd ed.; Saunders College: Fort Worth, TX; London, 1998; p 602.

self-assembly process for the first time. This research provides a new method to synthesize complicated nanotubular structures via simple self-assembly. The formation of microleaves and microtube dendrites shows solvent dependence. Micrometer-sized leaves and tube junctions and dendrites show semiconductor features, suggesting promising potential in nanodevice applications. Highly reproducible and sensitive gas response characteristics were observed in these microstructures. The applications of the dendrites arrays in sensors, photovoltaic cells, light-emitting display devices, and field emission devices are being explored.

Acknowledgment. Financial support from the Natural Science Foundation of China (Grant Nos. 20931001) and Ministry of Education of China is gratefully acknowledged.

Supporting Information Available: Electrochemical properties, IR spectra of the compound in the region 2700−3100 cm^{-1} with 2 cm^{-1} resolution, SEM images of the two-electrode device fabricated, $I-V$ curves measured on H_2T-$(C_{10}H_{21})_4P$ drop-cast film, AFM images of drop-cast film, SEM images of drop-cast film without solvent vapor annealing, AFM images of microtube dendrites, SEM images of microtube dendrites deposited for half a year, electronic absorption data for $H_2T(C_{10}H_{21})_4P$ in $CHCl_3$ and their self-assemblies annealed in solution vapor at quartz, and half-wave redox potentials of H_2T-$(C_{10}H_{21})_4P$ in CH_2Cl_2 containing 0.1 M TBAP. This material is available free of charge via Internet at http://pubs.acs.org.